Lecture 12. The diurnal cycle and the nocturnal BL

Over flat land, under clear skies and with weak thermal advection, the atmospheric boundary layer undergoes a pronounced diurnal cycle.   A schematic and an example from the Wangara experiment are shown on the next page. This 'archetypical' diurnal cycle is muted by clouds and can be entirely obscured by rapid changes in the free atmospheric conditions due for instance to the passage of a midlatitude cyclone or front. It is also highly modified by terrain or nearby land-sea contrasts. Despite these caveats, it is illuminating to study the archetypical case in more depth

During the night, the BL is stable due to surface longwave cooling, and a shallow temperature inversion of typically 100-500 m builds up. After dawn, surface heating builds up a shallow convective mixed layer, which deepens slowly and rapidly warms until it fully erodes the nocturnal stable layer. At this point, the top of the new mixed layer starts to penetrate into the **residual layer**, the remnants of the previous day's afternoon mixed layer. This layer is very weakly stratified, so the new mixed layer rapidly deepens into it, until it encounters the top of the previous day's mixed layer, which tends to be marked by a weak inversion. At this point, further BL warming occurs much more slowly, as a much deeper layer must be warmed than in the early morning. In the late afternoon, the solar heating is no longer sufficient to maintain upward surface buoyancy fluxes. Within an hour (a few eddy turnover times), turbulence collapses through most of the boundary layer and becomes restricted to a shallow layer, typically 100 m deep, driven by surface drag. During the night, clear-air radiative cooling is most intense near the cold surface, enhancing the static stability of the lowest couple of hundred meters of air. Much of the nocturnal inversion can be attributed to this cooling, rather than downward turbulent heat fluxes. However, downward heat fluxes of up to 50 W m^{-2} can occur near the surface at night under moderately strong geostrophic winds.
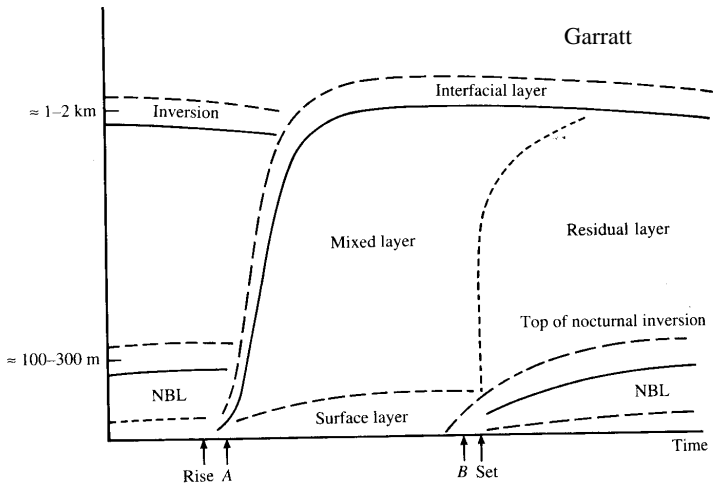
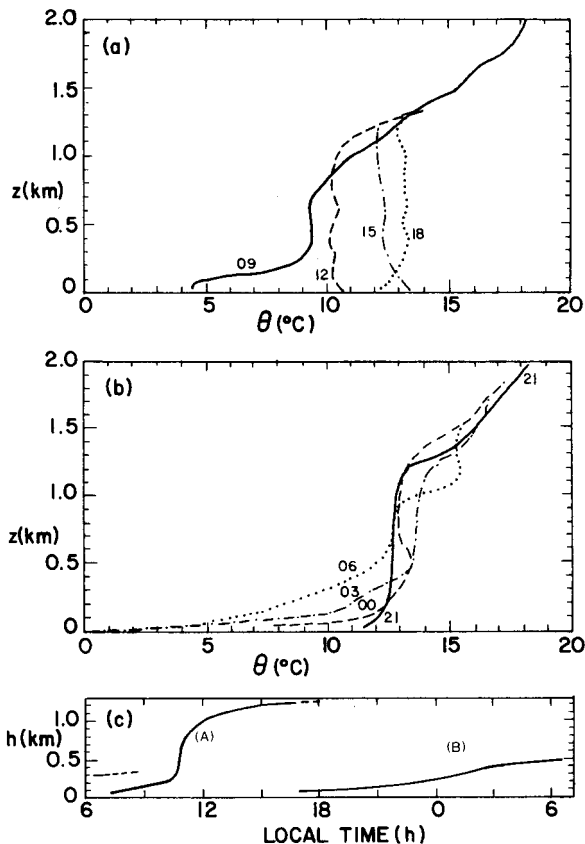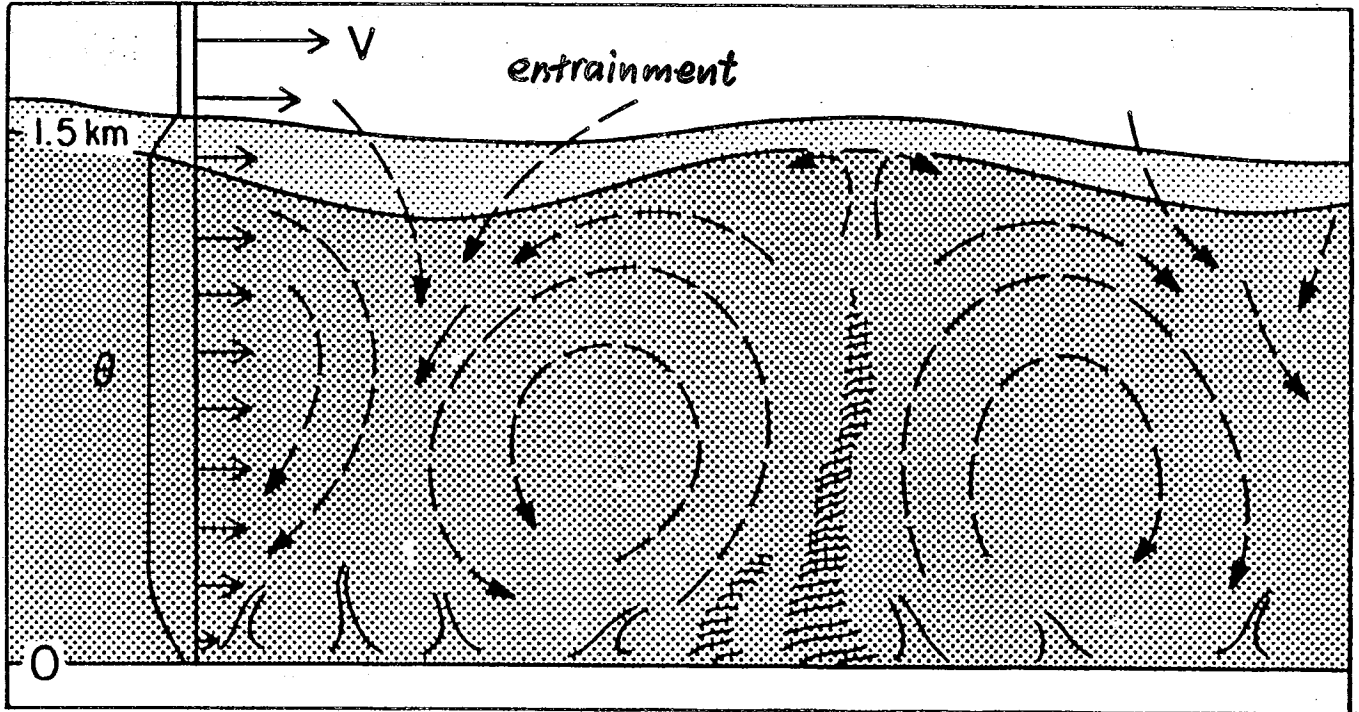Fig. 6.1 Schematic representation of ABL evolution throughout the diurnal period over land under clear skies.
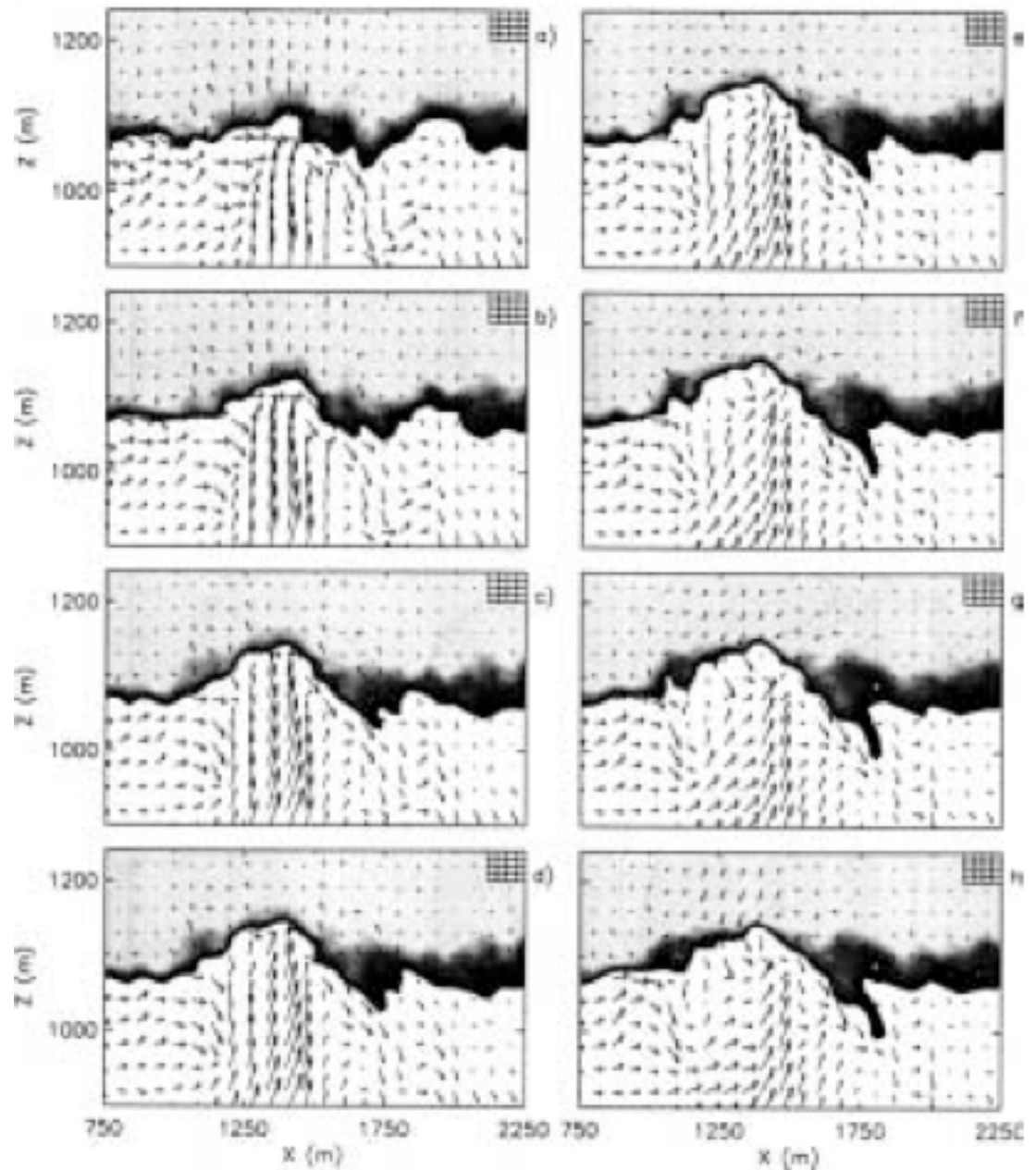
Arya

Fig. 5.2 Diurnal variation of potential temperature profiles and the PBL height during (a) day 33 and (b) days 33–34 of the Wangara Experiment. (c) Curve A, convective; Curve B, stable. [After Deardorff (1978).]

Convective Boundary Layer

V

entrainment

1.5 km

θ

0

LES-simulated entrainment event in a convective PBL

Sullivan et al. 1998

Atm S 547 Lecture 4, Slide

The rate of growth of the convective mixed layer is dictated primarily by energy balance, though entrainment dynamics also play a significant role. As a simple example, consider the growth of a mixed layer driven by a surface buoyancy flux B_0 into an atmosphere of constant buoyancy frequency N^2. The mean buoyancy profile in the free troposphere is

$b^+(z) = N^2 z$ $(= g(\theta_v^+(z) - \theta_{vR})/\theta_{vR}$, where we have chosen θ_{vR} as the initial θ_v^+ at $z = 0$.)

We assume (i) that the buoyancy flux is turned on at time $t = 0$, and (ii) that it leads to a convective mixed layer of depth $h(t)$ governed by the entrainment closure

$$\overline{w'b'}(h) = -w_e \Delta b = -\beta B_0 \quad (\beta = 0.2, \text{ empirically}) \tag{1}$$

It is interesting to compare the solution with a realistic β to the case $\beta = 0$. In the latter limit, called **encroachment**, convection is assumed not to be penetrative, and the mixed layer entrains air only when its buoyancy is no larger than that of the mixed layer air. Lastly, (iii) we neglect any mean vertical motion within the atmosphere, so

$$w_e = dh/dt$$

The buoyancy $b(z, t)$ obeys

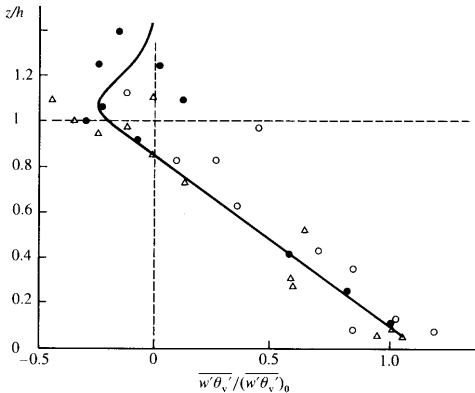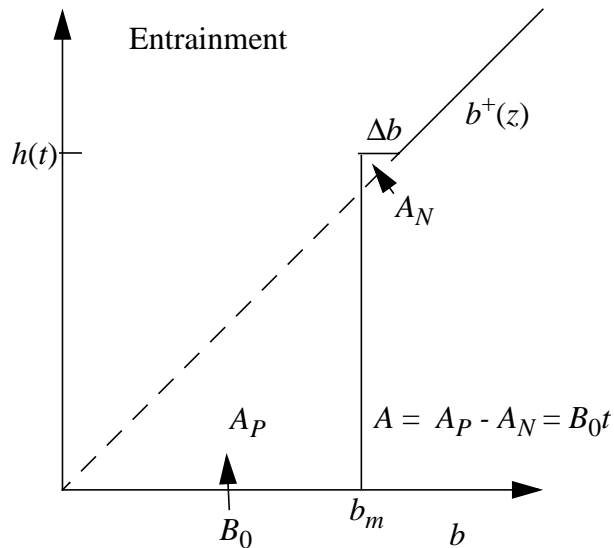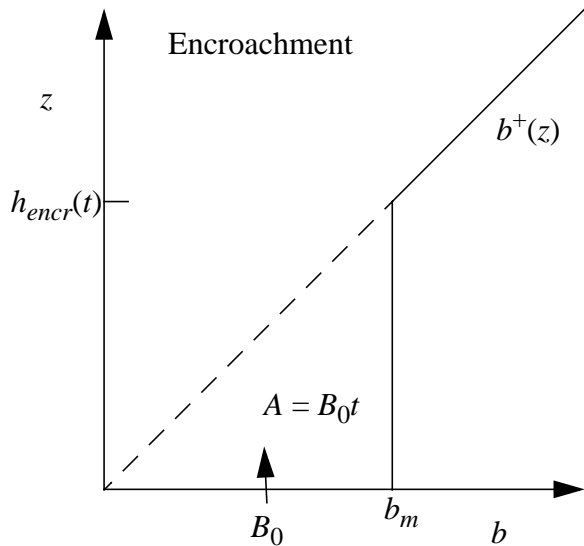$$\partial b/\partial t = -\partial/\partial z(\overline{w'b'})$$

Fig. 6.2 Experimental data on the vertical variation of the virtual heat flux, normalized by its surface value; h is the depth of the mixed layer. Data are for three days from the 1983 ABL experiment; see Stull (1988, Figs. 3.1, 3.2 and 3.3). See also Fig. 6.23 of this volume.

In a convective BL, entrainment buoyancy flux is $-0,2B_0$

Convective mixed layer evolution illustrating more rapid deepening if entrainment is assumed to be penetrative ($\beta = 0.2$), compared to encroachment ($\beta = 0$).

Integrating from the surface up to a fixed height H above the mixed layer top, we see that

$$\frac{\partial}{\partial t}\int_0^H b\, dz = -\overline{w'b'}\Big|_0^H = B_0$$

Graphically, let A be the net area added to the buoyancy profile by the heating of the BL. Then

$$A = B_0 t \tag{2}$$

We can now compare the cases of encroachment and an entraining boundary layer. The encroaching BL has depth given by

$$h(N^2 h)/2 = A = B_0 t \quad \Rightarrow \quad h_{encr} = (2B_0 t/N^2)^{1/2}$$

As expected, h deepens more slowly as it gets larger, since more heat must be imparted to a deeper boundary layer to raise its buoyancy by a given amount.

For the entraining BL, there is a 'similarity' solution in which the buoyancy profile retains the same shape as it grows, so that

$$\Delta b(t) = cN^2 h(t) \quad (c \text{ is an as yet unknown constant}).$$
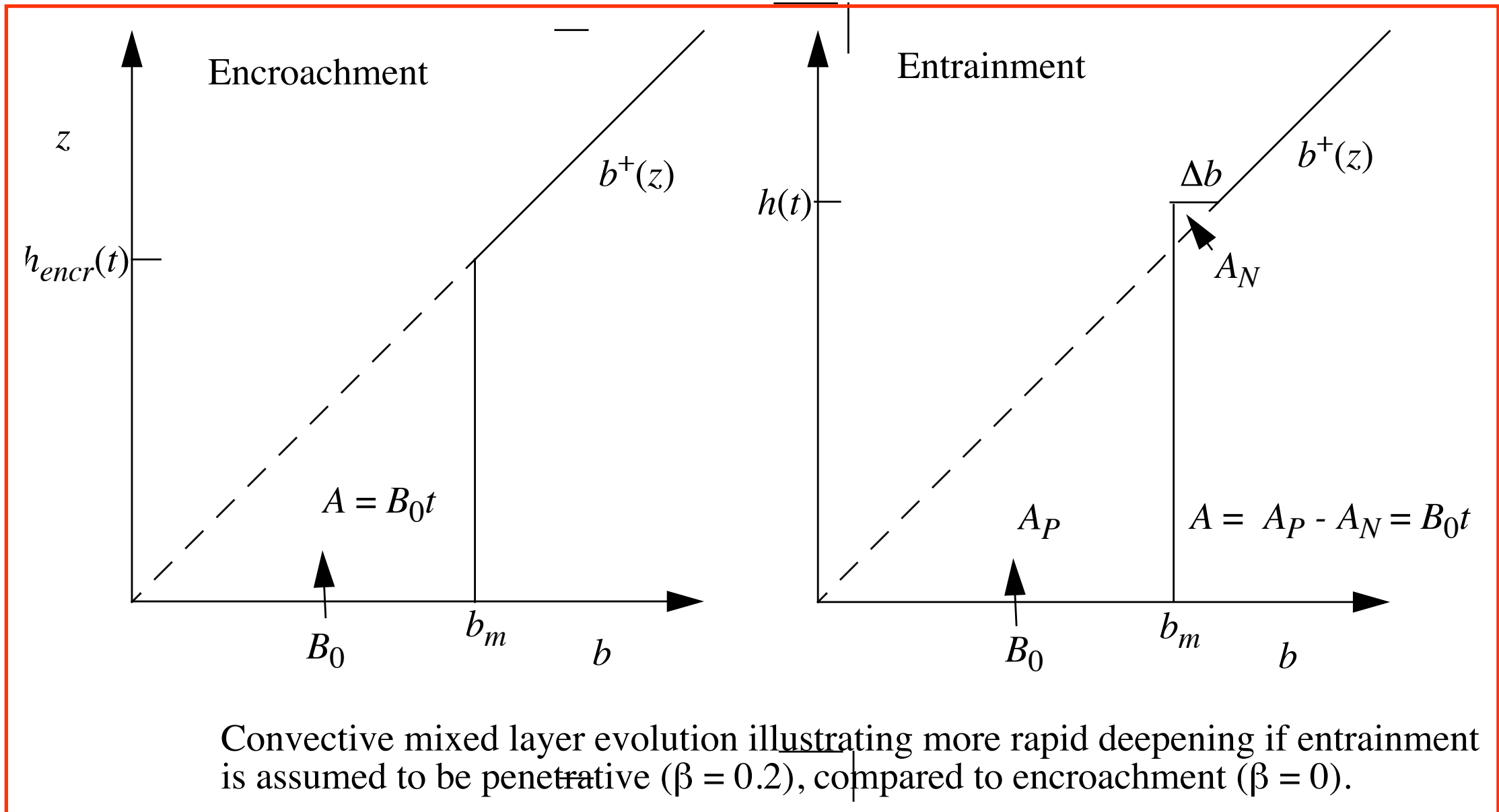
Consistency of (1) and (2) determines c. From (1),

$$\beta B_0 = w_e \Delta b = (dh/dt)cN^2 h.$$

Integrating this equation from time 0 to t, starting with $h(0) = 0$, we get

$$\beta B_0 t = cN^2 h^2/2 \tag{3}$$

Convective mixed layer evolution illustrating more rapid deepening if entrainment is assumed to be penetrative ($\beta = 0.2$), compared to encroachment ($\beta = 0$).

Graphically, let A be the net area added to the buoyancy profile by the heating of the BL. Then

$$A = B_0 t \qquad (2)$$

Turning now to (2), we write A as the difference of the 'positive area' A_P where the mixed layer buoyancy $b_m(t)$ exceeds the original environmental buoyancy and the negative area A_N where penetrative convection has reduced the buoyancy. From the figure above, we see that $b_m + \Delta b = b^+(t) = N^2 h$, so $b_m = (1-c)N^2 h$. The heights of the triangles making up A_P and A_N are N^{-2} times as long as their bases, so the area of A_P is $b_m(b_m/N^2)/2$ and similarly for A_N. Hence (2) can be written:

$$B_0 t = A = A_P - A_N = b_m^2/2N^2 - \Delta b^2/2N^2 = [(1-c)^2 - c^2]N^2 h^2/2 = (1 - 2c)N^2 h^2/2. \qquad (4)$$

Dividing (3) by (4), we see that $\beta = c/(1 - 2c)$, or that $c = \beta/(1 + 2\beta)$. It follows from (4) that

$$h_{entr} = (2B_0t/N^2(1 - 2c))^{1/2} = (2B_0t(1 + 2\beta)/N^2)^{1/2} \approx (1 + \beta)h_{encr}$$

We conclude that entrainment contributes about $\beta = 20\%$ to the boundary layer deepening. For a 1 km deep BL and $N^2 = 10^{-4}$ s^{-1}, the inversion strength would be $\Delta b = .14N^2h \leftrightarrow \Delta\theta_v \approx 0.4$ K, regardless of the surface buoyancy flux. Entrainment hardly changes the boundary layer temperature.

As turbulence dies down in the residual layer in late afternoon, it decouples from the BL. The momentum flux convergence that was helping to reduce and turn the wind during the day suddenly disappears, leaving a wind profile in which there is an imbalance between the two main horizontal

forces, Coriolis force and pressure gradient force. The figure below shows the resulting evolution of the wind during one night of the Wangara experiment (which took place over flat ground). During the night a strong jet develops above the nocturnal BL. In the bottom panel is another example in which the geostrophic wind is also plotted. During the daytime, the wind component along the geostrophic wind direction is subgeostrophic, but at night it is supergeostrophic.

This is one of the cleanest atmospheric examples of an inertial oscillation. The pressure gradient is horizontally uniform, so the ageostrophic wind $\mathbf{u}_a = \mathbf{u} - \mathbf{u}_g$ rotates clockwise with the Coriolis period $2\pi/f$, which at mid-latitudes is somewhat less than a day. Supergeostrophic winds ensue dur-
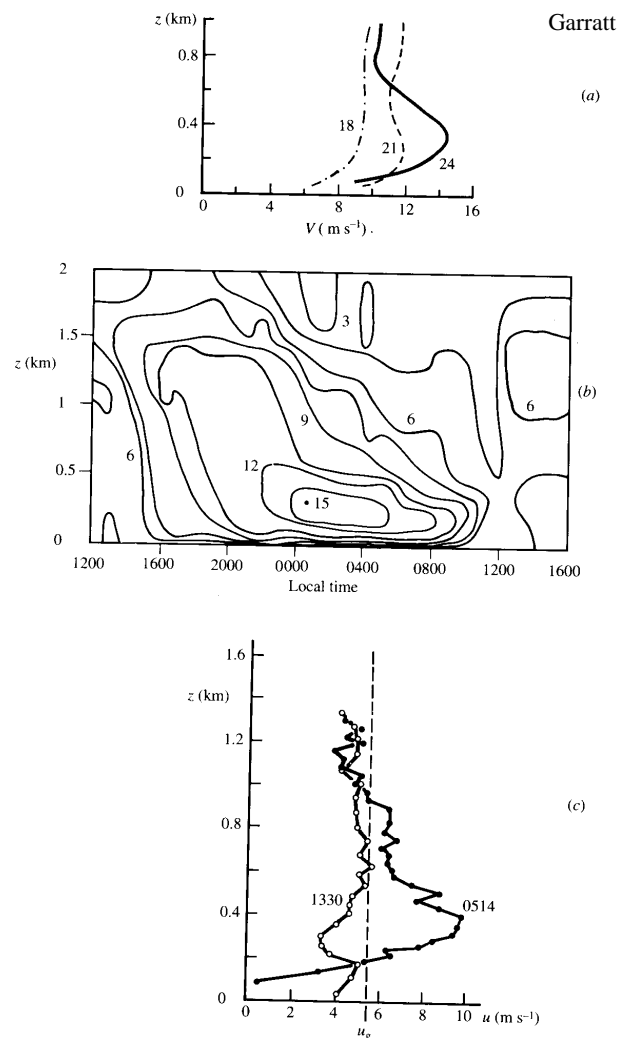

Fig. 6.18 Observations illustrating the formation of the nocturnal jet. (a) Wind-speed profiles on day 13 of WANGARA, local times indicated. (b) Height–time cross-section of wind speed (in m s^{-1}) on days 13/14 at WANGARA. Isopleths of wind speed are drawn at 1.5 m s^{-1} intervals. (c) Profiles of the u-component of the wind velocity, with the x-axis along the geostrophic wind direction, for mid-afternoon (1330 UT, 6 August, 1974) and early morning (0514, 7 August, 1974) near Ascot, England. After Thorpe and Guymer (1977), *Quarterly Journal of the Royal Meteorological Society*.
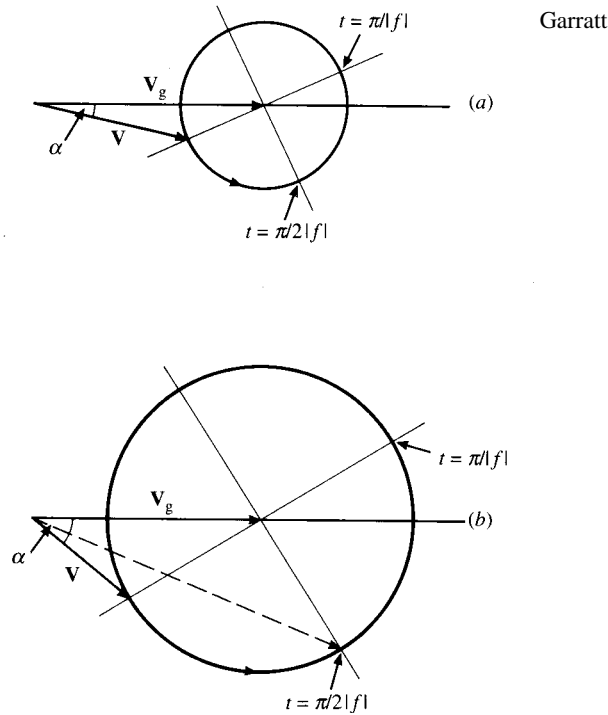
Fig. 6.19 Illustrated solutions of the unbalanced momentum equation (Eq. 6.77) for (*a*) a low-roughness surface and (*b*) a high-roughness surface; undamped inertial oscillations are shown for the southern hemisphere in the form of anticlockwise rotation of the wind vector (**V**) about the geostrophic wind vector (**V**$_g$).

ing the night , as shown in the figure above.   In the morning, the convective mixed layer deepens into the residual layer, so the wind profile becomes frictionally coupled again. The Great Plains nocturnal southerly jet, prominent during the springtime when it can achieve speeds of 30 m s^{-1} less than 1 km above the surface, partially owes its origin to this mechanism. In this region, climatological southerly geostrophic flow occurs due to a thermal low over the elevated terrain to the west (i. e. the Rockies). The strong enhancement of low-level southerlies during the night help pump humid air northward, where it can help fuel severe thunderstorms and mesoscale convective systems through the night.